Seismic Fault-induced Failures, 101-108, 2001 January

LAGRANGIAN PARTICLES FOR MODELING LARGE SOIL DEFORMATIONS

K. KONAGAI[1] and J. JOHANSSON[2]

[1]Dr. Eng., Professor, Institute of Industrial Science, University of Tokyo.
(4-6-1 Komaba, Meguro-Ku, Tokyo 153-8505, Japan, konagai@iis.u-tokyo.ac.jp)
[2]Ph. D. Candidate, Institute of Industrial Science, University of Tokyo.
(4-6-1 Komaba, Meguro-Ku, Tokyo 153-8505, Japan, jorgen@iis.u-tokyo.ac.jp)

A Lagrangian Particle Finite Difference Method (LPFDM) is presented for analyzing large deformations of soils. By introducing the concept of Lagrangian material points into a FDM or FEM, numerical problems related to large deformations can be avoided. The material points move with the material and carry all necessary information, which for each time step is mapped back and forth between the points and a grid where the equations of motion are solved. LPFDM describes on a Eularian grid solid motions obtained through a simple Gaussian calculation scheme similar to FLAC. The method thus retains the merits of FLAC avoiding mesh distortion and convection problems.

Key Words : *Large deformations, Lagrangian particle method, Eulerian lattice, MPM, FLAC, fault-inflicted damage, grain inclusion, PSC test*

1. INTRODUCTION

The 1999 Kocaeli and Duzce Earthquakes, Turkey, and Chi-Chi Earthquake, Taiwan, have raised the need to reduce the fault-inflicted damage to structures, a formidable problem demanding a lot of research and discussions. In some less populated regions, limiting the development within active fault zones would be very effective; In California, USA, such a law was enacted already in the early 1970's This limitation, however, is a very difficult implement especially in overpopulated countries such as Taiwan and Japan. Moreover, soil deformation is not always localized just on a particular fault rupture plane, but can be distributed within a certain band along the fault. To discuss plausible remedial measures, it is necessary to study the possible extent of the very large plastic deformations taking place in soil deposits on top of faults (Bray, 1990). For such studies, suitable numerical tools are necessary.

For studying large deformations of soils, numerical methods such as FEM or FDM have been widely used. For example, the finite difference based FLAC (Fast Lagrangian Analysis of Continua, Cundall, 1979) successfully calculates large strains by using low-order strain elements. However, when dealing with large strains, highly distorted elements often account for inaccurate results. In the field of computational fluid dynamics, where history-dependent materials are less common, purely Eulerian methods are often used. To model highly distorted flows, Harlow (1964) introduced the partially Lagrangian Particle-In-Cell method (PIC). Unfortunately, it had high numerical dissipation, and to avoid this problem, Brackbill et al. (1988) developed the fully Lagrangian method, FLIP (Fluid Lagrangian Implicit Particle). It uses particles to model convection as in PIC, but it was extended to model the fluid during the whole calculation cycle. Later, Burgess et al. (1992) included a global consistent mass matrix into the FLIP method to reduce the so-called "ringing" instability, and Sulsky et al. (1994) extended it further to solid mechanics. The method is now referred to as the Material Point Method (MPM). In the MPM material points move through the cells of a computational mesh carrying all the necessary Lagrangian parameters such as mass, stress, strain, position, strength etc. Any mesh type could be chosen to suit a typical problem, but a fixed Eulerian mesh is easiest to use. The method thus takes advantage of both Eulerian and Lagrangian features, by avoiding mesh distortion and convection problems.

In an ongoing effort by the authors to develop numerical tools based on MPM for modeling large deformations of soil and other civil engineering materials, a simpler method based on a finite difference scheme has been developed. The LPFDM (Lagrangian Particle Finite Difference Method) presented herein is similar to FLAC in that constant strain increment elements are used but the increments are more rationally computed with the use of Gauss's divergence theorem. The present finite difference scheme, in which a global mass matrix is not calculated, is very fast and can be adapted to arbitrarily-shaped cells without changing the basic descriptions of the formulation. Like the MPM, LPFDM allows for adaptive meshing.

2. LAGRANGIAN POINT FINITE DIFFERENCE METHOD (LPFDM)

2.1. Calculation scheme

LPFDM embodies an explicit time-marching scheme, while implicit, matrix-oriented solution schemes are more common in finite element methods. All Lagrangian variables are carried by unconnected Lagrangian material points (See **Figure 1**); the points, as a cluster, describe the mass of the material. An Eulerian mesh is used to solve the equations of motion in each time step. Lagrangian parameters of all material points included in one cell of the mesh contribute to the cell's nodes, and accelerate them. As a consequence, the cell deforms carrying the material points with it, but it is shifted back to its original position for the next calculation cycle.

Assuming that the updated nodal displacements are know, strain increments in a cell can be obtained by using Gauss's divergence theorem. For an area A enclosed by a surface S, Gauss's divergence theorem has the following form in the Cartesian coordinate system as:

$$\int_S n_j u ds = \int_A \frac{\partial u}{\partial x_j} dA \qquad (1)$$

where,

$\int_S ds$ is the integral along the boundary S of a closed area A;

n_j $= \mathbf{n} \cdot \mathbf{j}$; Here $\mathbf{n}$ and $\mathbf{j}$ are unit vectors normal to the surface S and along the direction of x_j axis, respectively;

x_j can be either x or y in the Cartesian co-ordinate system (x, y);

u can be a scalar, vector or tensor; and

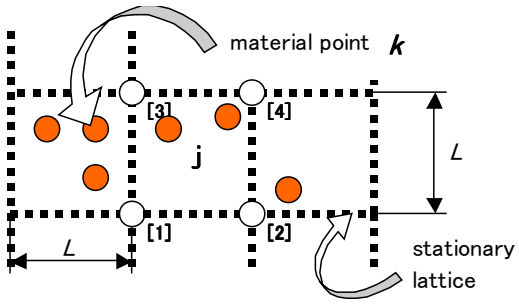

Figure 1. Stationary lattice and material points

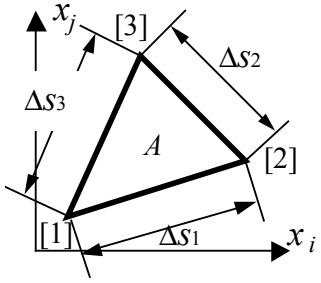

Figure 2 Triangular cell

$\int_A dA$ is the integral over the area A.

Defining the average value of the gradient over the area as:

$$\left\langle \frac{\partial u}{\partial x_j} \right\rangle = \frac{1}{A} \int_A \frac{\partial u}{\partial x_j} dA \qquad (2)$$

one obtains from Equation (1):

$$\left\langle \frac{\partial u}{\partial x_j} \right\rangle = \frac{1}{A} \int_S n_j u ds \qquad (3)$$

When the closed area is a triangle as shown in **Figure 2**, and u is assumed to vary linearly along each side, the following finite difference formulae is obtained:

$$\left\langle \frac{\partial u}{\partial j} \right\rangle = \frac{1}{A} \sum_{k=1}^{3} \langle u \rangle_k n_j \Delta s_k \qquad (4)$$

where, the summation is over the three sides, and $\langle u \rangle_k$ is the average value of u over the side k.

Keeping in mind that $n_j \Delta s_k$ is the projection of Δs_k on x_i axis, Equation (4) for the triangle in **Figure 2** is rewritten as:

$$\left\langle \frac{\partial u}{\partial x_j} \right\rangle = \frac{1}{A} \{ \frac{u^{[1]} + u^{[2]}}{2} \cdot (x_i^{[1]} - x_i^{\{2]}) + \frac{u^{[2]} + u^{[3]}}{2} \cdot (x_i^{[2]} - x_i^{[3]}) + \frac{u^{[3]} + u^{[1]}}{2} \cdot (x_i^{[3]} - x_i^{[1]}) \} \qquad (4a)$$

or

$$\left\langle \frac{\partial u}{\partial x_j} \right\rangle = \frac{1}{2A}\left\{ u^{[1]}\left(x_i^{[1]} - x_i^{[2]}\right) + u^{[2]}\left(x_i^{[2]} - x_i^{[3]}\right) + u^{[3]}\left(x_i^{[3]} - x_i^{[1]}\right)\right\} \quad (4b)$$

with $$A = \frac{1}{2}\begin{vmatrix} 1 & x_i^{[1]} & x_j^{[1]} \\ 1 & x_i^{[2]} & x_j^{[2]} \\ 1 & x_i^{([3]} & x_j^{[3]} \end{vmatrix}$$

where, superscripts [1], [2], [3] denote local nodal point numbers in **Figure 2**.

Equation (4) can be used for any arbitrarily-shaped polygon to describe the strain increments in terms of the nodal displacement increments by simply replacing u with $\Delta u^{[k]}$. In LPFDM, a regular square mesh with sides parallel to x and y axes of the Cartesian co-ordinate system is used (**Figure 1**). Replacing in Equation (4b) x_i and x_j with x and y, and increasing the node number to 4, the strain increment of j-th element is obtained as:

$$\left(\Delta\varepsilon_{xx}\right)_j = \frac{\left(\Delta u_x^{[2]} + \Delta u_x^{[4]} - \Delta u_x^{[1]} - \Delta u_x^{[3]}\right)_j}{2L} \quad (5a)$$

$$\left(\Delta\varepsilon_{yy}\right)_j = \frac{\left(\Delta u_y^{[3]} + \Delta u_y^{[4]} - \Delta u_y^{[1]} - \Delta u_y^{[2]}\right)_j}{2L} \quad (5b)$$

$$\left(\Delta\varepsilon_{xy}\right)_j = \frac{\left(\Delta u_x^{[3]} + \Delta u_x^{[4]} - \Delta u_x^{[1]} - \Delta u_x^{[2]}\right)_j}{2L} \quad (5c)$$

$$\left(\Delta\varepsilon_{yx}\right)_j = \frac{\left(\Delta u_y^{[2]} + \Delta u_y^{[4]} - \Delta u_y^{[1]} - \Delta u_y^{[3]}\right)_j}{2L} \quad (5d)$$

where L is the cell side length.

The shear strain increment $\Delta\gamma_{xy}$ satisfies:

$$\left(\Delta\gamma_{xy}\right)_j = \left(\Delta\varepsilon_{xy}\right)_j + \left(\Delta\varepsilon_{yx}\right)_j \quad (5e)$$

and rotational increment $\Delta\theta$ is given by:

$$\left(\Delta\theta\right)_j = \frac{1}{2}\left(\Delta\varepsilon_{yx} - \Delta\varepsilon_{xy}\right)_j \quad (5f)$$

All material points included in Cell j are assumed to experience the same strain increments given by equations (5a)-(5f).The location of material point k $\{x(k), y(k)\}$ in the cell j deformed at the preceding time step is updated as:

$$x(k) \Leftarrow x(k) + \Delta u_x^{[1]} \cdot \left(1 - \frac{\Delta x(k)}{L}\right)\left(1 - \frac{\Delta y(k)}{L}\right) + \Delta u_x^{[2]} \cdot \frac{\Delta x(k)}{L}\left(1 - \frac{\Delta y(k)}{L}\right) + \Delta u_x^{[3]} \cdot \left(1 - \frac{\Delta x(k)}{L}\right)\frac{\Delta y(k)}{L} + \Delta u_x^{[4]} \cdot \frac{\Delta x(k)}{L}\frac{\Delta y(k)}{L}$$

$$y(k) \Leftarrow y(k) + \Delta u_y^{[1]} \cdot \left(1 - \frac{\Delta x(k)}{L}\right)\left(1 - \frac{\Delta y(k)}{L}\right) + \Delta u_y^{[2]} \cdot \frac{\Delta x(k)}{L}\left(1 - \frac{\Delta y(k)}{L}\right) + \Delta u_{yx}^{[3]} \cdot \left(1 - \frac{\Delta x(k)}{L}\right)\frac{\Delta y(k)}{L} + \Delta u_y^{[4]} \cdot \frac{\Delta x(k)}{L}\frac{\Delta y(k)}{L} \quad (6a), (6b)$$

where,

$\Delta x(k)$= $x(k)$ - (x-coordinate of node [1] of Cell j)

$\Delta y(k)$= $y(k)$ - (y-coordinate of node [1] of Cell j).

When all the Lagrangian variables are updated at all material points, the Eulerian grid is shifted back to its original position for the following calculation cycle. To solve the equation of motion at the grid nodes the following parameters are obtained by mapping form the material points.

The mass of each cell is obtained by adding up all the masses of material points included in the cell j:

$$\left\langle M \right\rangle_j = \sum_{k \in j} m_k \quad (7)$$

Here, it is noted that a set of material points included in the cell j has also been updated.

The stresses for each material point are obtained from the specific constitutive model. For the explicit scheme used in LPFDM, the constitutive law is only consulted once per material point during one time step. The stress is smeared over the cell:

$$\left\langle \sigma \right\rangle_j = \left\{ \sum_{k \in j} \frac{m_k}{\rho_k} \sigma(k) \right\} / L^2 \quad (8)$$

where, the quotient of material point mass and density m_k / ρ_k is the volume of the material point k. In order to obtain the nodal forces at node [k] of Cell j (see **Figure 1**), a virtual unit displacement is applied to node [k]. The stress components $\left\langle \sigma \right\rangle_j$ smeared over the cell j must perform the same amount of work done by the nodal forces $F_i^{[k]}$ ($i = x$ or y): this calls for;

$$F_i^{[k]} = \frac{\left\langle \sigma_{ii} \right\rangle (x_j^{[k-1]} - x_j^{[k+1]})}{2} + \frac{\left\langle \sigma_{ij} \right\rangle (x_i^{[k-1]} - x_i^{[k+1]})}{2} \quad (9)$$

where, $(x_i \quad x_j)$ is either $(x \quad y)$ or $(y \quad x)$.

At each node (global node number = (k)), the forces from all surrounding cells (elements) are summed up to give the net nodal force;

$$F^{(k)} = \sum_{[k] \in (k)} F_i^{[k]} \quad (i = x \text{ or } y). \quad (10)$$

This vector includes contributions from applied loads and body forces due to gravity. Gravity forces are computed from:

$$F_{g,i}^{(k)} = g_i m^{(k)} \quad (11)$$

where $m^{(k)}$ is the lumped mass at the node (k), defined as 1/4 of the masses of the cells connected to the node. If a connected cell does not contain any material point, its contribution to the nodal force is omitted. The nodal force accelerates the lumped mass, and the acceleration is integrated to obtain the nodal displace increment:

$$\Delta u_i^{(k)}(t + \Delta t/2) = \Delta u_i^{(k)}(t - \Delta t/2) + \frac{\Delta t^2}{m^{(k)}} F_i^{(k)} \quad (12)$$

Since a Eulerian grid is used in the LPFDM, a convection term should be added to Equation (12).

The convection is compensated for with the following procedure:

$$\Delta u_x^{(k)}(t-\Delta t/2) \Leftarrow \Delta u_x^{(k)}(t-\Delta t/2)\cdot\left(1-\left(\Delta\varepsilon_{xx}\right)_{j^{(k)}}\right)-\Delta u_y^{(k)}(t-\Delta t/2)\cdot\left(\Delta\varepsilon_{xy}\right)_{j^{(k)}}$$

$$\Delta u_y^{(k)}(t-\Delta t/2) \Leftarrow \Delta u_y^{(k)}(t-\Delta t/2)\cdot\left(1-\left(\Delta\varepsilon_{yy}\right)_{j^{(k)}}\right)-\Delta u_x^{(k)}(t-\Delta t/2)\cdot\left(\Delta\varepsilon_{yx}\right)_{j^{(k)}}$$

(13a),(13b)

where, $j^{(k)}$ is the cell in which the previous mark of nodal point (k) on the material is found.

When quasi-static behaviors are concerned, the motions of nodes are damped with minimal computational effort. A form of artificial damping, called local non-viscous damping (Cundall, 1987), is used in *LPFDM* in which the damping force on a node is proportional to the magnitude of the unbalanced force. The direction of the damping force is taken in such a way that energy is always dissipated. Equation (12) is thus replaced with the following equation:

$$\Delta u_i^{(k)}(t+\Delta t/2)=\Delta u_i^{(k)}(t-\Delta t/2)+\frac{\Delta t^2}{m_k}\left(F_i^{(k)}-D_i^{(k)}\right) \quad (14)$$

where, $D_i^{(k)}=\alpha\left|F_i^{(k)}\right|\mathrm{sgn}(\Delta u_i^{(k)}(t-\Delta t/2))$ (15)

$D_i^{(k)}$ is the damping force, α is a constant.

2.2. Necessary items

A fixed mesh, in an arrangement of $mx \times my$ square cells with "***nodal points***", is used to describe the locations of "***Lagrangian points***" (**Figure 3**). Areas of the lattice filled with Lagrangian points are referred to as "***clusters***". Initially, the Lagrangian points are arranged in square in each cell of a cluster**.**

In addition to the above mentioned items, "***moving walls***" are introduced into LPFDM. A *moving wall* is realized by giving all designated nodes lined up on the lattice the same displacement increments at once. When the accumulation of the increments given to each node reaches one cell size, the displacement increments are given to the next line of nodes.

3. SIMULATIONS

The soil is assumed to be elasto-plastic, obeying the simple Mohr-Coulomb's yield criterion. Once the peak strength is reached in one Lagrangian point, chemical bonds or granular fabrics among grains are assumed to be broken causing the cohesion to be reduced to some prescribed extent. **Table 1** shows the parameters for the material used in the examples.

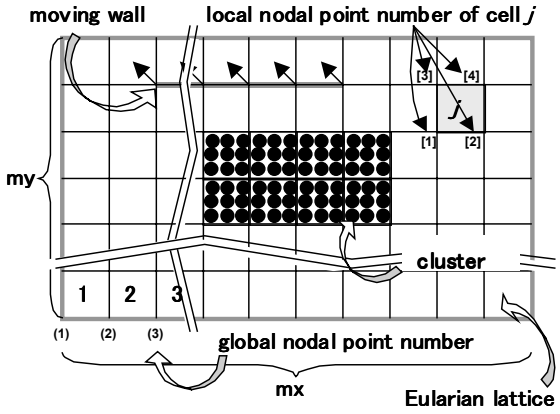

Figure 3. Necessary items in LFPDM.

Table 1. Mechanical properties

Young's modulus:	5×10^7 N/m^2
Poisson's ratio:	0.47
Density:	1700 kg/m^3
Internal friction angle:	0.5 rad
Cohesion:	9800 N/m^2
Strength reduction:	Cohesion is reduced by 50%

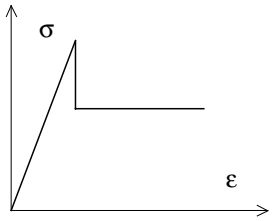

Figure 4 Assumed Stress-strain curve for a material point

Both the internal friction angles and the cohesions for Lagrangian points were given a Gaussian distributions with mean values given in **Table 1** and a standard deviation of 25% for the following simulations **(3)** and 33% for the others. The shape of typical stress-strain curve for a Lagrangian point is shown in **Figure 4**.

(1) *Failure of steep slope*

Figure 5 shows a soil mass that collapses under its own weight. The α variable was set at 0.8 in Equation (15) for the local non-viscous damping. Despite the coarse discretization ($L=1$m), detailed features of this cliff failure were vividly described. Initially the deformation is slow, but as plastic strains begin to accumulate, certain regions become softened and rapid shear-band formation occurs from the toe up through the cliff. The corner wedge of the soil mass then starts sliding down the softened slope, being accompanied by a secondary shear-band formation just behind the scar.

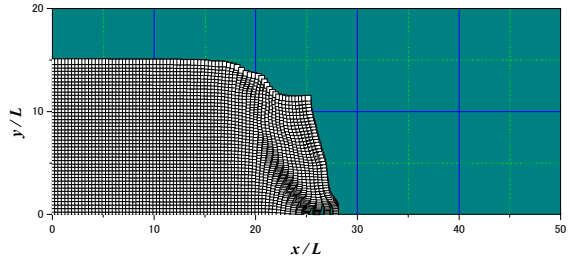

(a) 2.5s

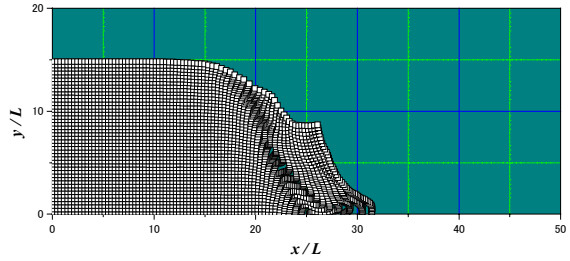

(b) 5.0s

Figure 5 Simulation of cliff failure ($\Delta t = 0.0005s$)

(2) *Mass Flow through a Trap door*

A mass flow through a trap door was simulated (**See Figure 6)**. The internal friction angle was set at 0.0 for this simulation; except that, mechanical properties are the same as those listed in **Table 1**. The gravitational acceleration was given at once to the mass, and the mass started flowing under its own weight. The opening of the door is just twice the cell size L, and yet, the mass exhibiting a noticeably flexible nature can flow through the narrow opening. In the second simulation (**Figure 7**), an obstacle was placed right above the trap door. One can see that the soil flows past the obstacle and through the trap door. Some flow stagnation occurs around the obstacle.

(3) *Plane-Strain Compression Tests*

Since the objective of the research is to obtain the possible extent of fault-induced soil deformations, appropriate constitutive models are necessary for the surface soils. Along faults, alluvial deposits including large boulders are often found. To see how these large inclusions in a soil matrix affect the soil's overall behavior, an extensive study will be performed and addressed in a later publication. To demonstrate the potential of the Lagrangian particle technique, some examples of PSC test with inclusions of large grains/boulders follow below.

Figure 8 shows the simulation of a plane-strain compression test on a soil with the properties given in **Table 1**. In order to compress the specimen, a

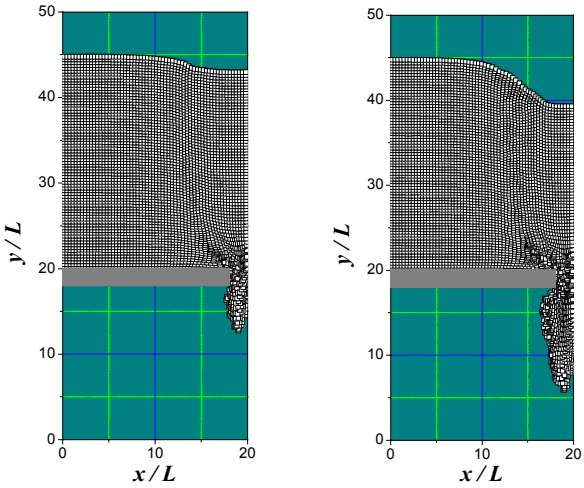

(a) 2.5s **(b)** 5.0s

Figure 6 Mass flow through a trapdoor ($\Delta t = 0.0005s$)

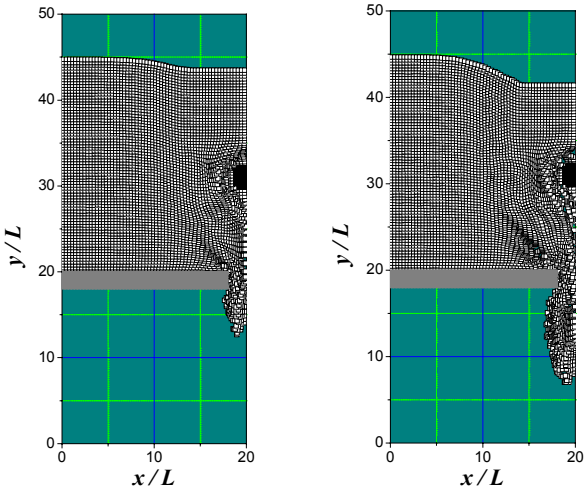

(a) 2.5s **(b)** 5.0s

Figure 7 Mass flow through a trapdoor with an obstacle right above ($\Delta t = 0.0005s$)

stiff cap was put immediately above the top end of the specimen, and was slowly driven down at a constant velocity. The confining pressure was zero. In the figures, both the height and width of the specimen are normalized by the cell width L. and material points were initially arranged in 4×4 square in each cell. The stress was measured at the bottom of the specimen.

Though each material point has simple mechanical features as described in **Table 1**, the overall deviatoric stress-strain relationship (**Fig. 8a**) exhibits rather realistic curvature. This is because the values given in **Table 1** were given random

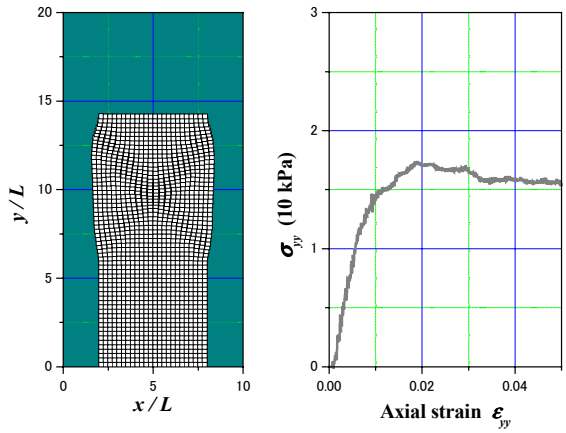

(a) No grain inclusion

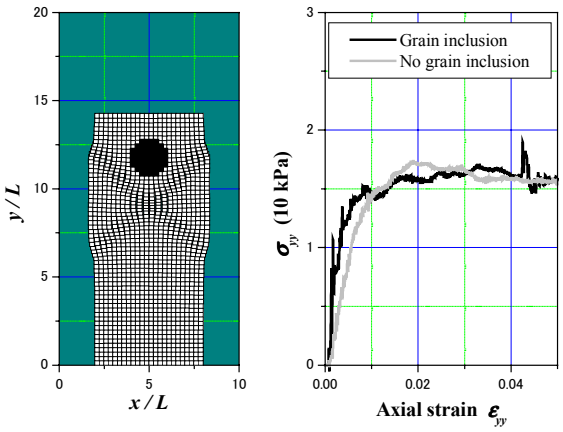

(b) Grain location: 2.5*L* below the top

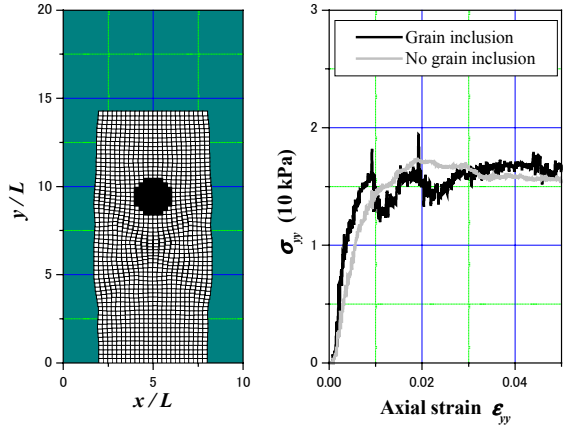

(c) Grain location: 5.0*L* below the top

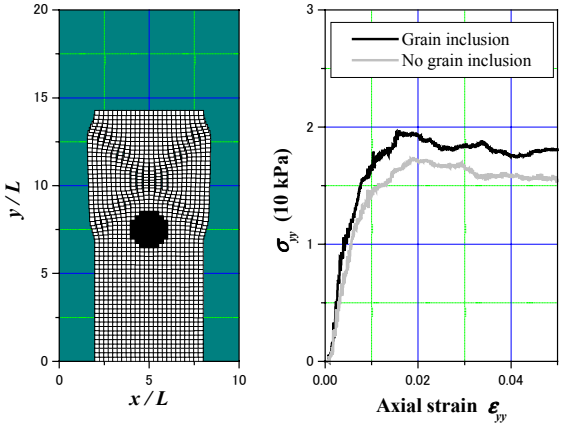

(d) Grain Location: 7.5*L* below the top

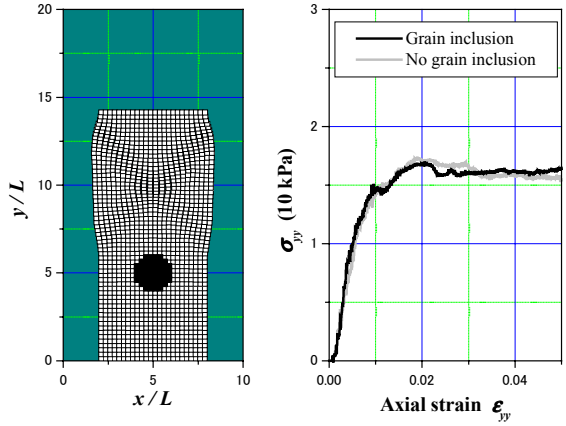

(e) Grain Location: 10.0*L* below the top

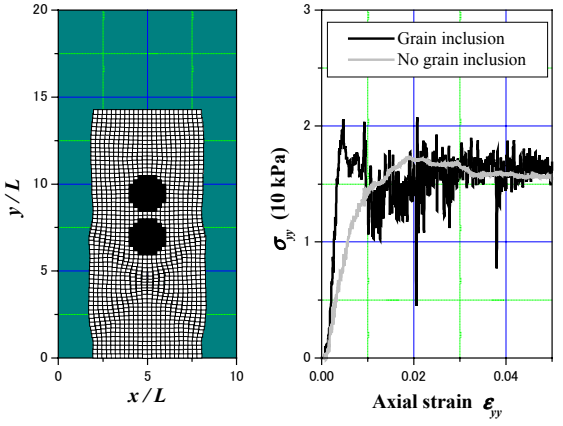

(f) Two grain inclusions: 5.0L & 7.5L below the top

Figure 8 PSC test simulations

deviation and the strain is the ratio of cap displacement and the height of the specimen. Two diagonal shear bands can be seen across the specimen. The shear-band width is strongly affected by the cell size *L* because strain increments are assumed to be equally distributed over each cell. **Figures 8b-8f** show the PSC tests results of specimens with grain inclusions. A perfect bonding is assumed between the grain and the soil matrix. As can be seen, the shear bands avoid the inclusion and form below the grain in **(b)** and **(c)**, but with the grains placed further down, the shear bands can form at the top of the specimen. When the shear bands form below the grain, the stress-strain curves fluctuate, whereas it is smoother when the shear band forms above the grain.

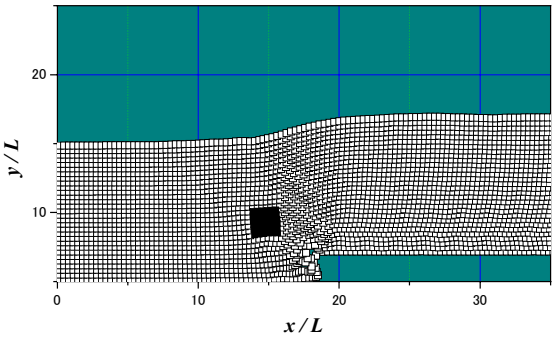

(a) Vertical offset = 3.75*L*

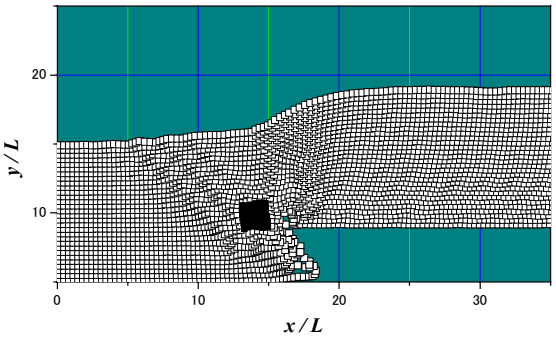

(b) Vertical offset = 7.5*L*

Figure 9 Reverse faulting
(Internal friction angle = 0)

(4) *Reverse Faulting*
To estimate quantitatively the possible extent of soil deformations caused by faulting, numerical simulations are necessary. **Figure 9** shows a simple simulation of a reverse faulting with a stiff square inclusion. The base rock coming steadily up in the surface soil gradually pushes the grain aside, and when the vertical offset reaches 7.5 cell size (**Figure 9b**), it can be seen that the square inclusion causes some shear bands to develop diagonally up through the soil deposit, and makes an appearance of some small bumps upon the soil surface. These fault simulations will be extended to include underground structures such as tunnels and pipelines or bridge abutments, and addressed in later publication.

4. LPFDM vs FLAC, MPM, FEM

The LPFDM presented herein is similar to FLAC in that constant-strain increment elements are used. FLAC however uses an overlay scheme, in which a quadrilateral element is modeled as two overlaid pairs of constant-strain triangles. The forces exerted on each node are taken to be the mean of those exerted by the two quadrilaterals, and strains are eventually smeared over the quadrilateral (Mixed-discretization procdure; Marti and Cundall, 1982). The overlay scheme thereby ensures isotropy, and successfully restrains hourglass deformations. The procedure, however, is not appropriate especially when the quadrilateral is badly distorted and paired triangles' areas are considerably out of balance. As contrasted with FLAC, hourglass deformations do not occur in LPFDM simulations because a fixed Eularian grid is used; hence the overlay scheme is not taken in LPFDM allowing strains to be more rationally computed

In the present scheme of the LPFDM, a convection term has to be added to a solution for the updated nodal values. This convection term is avoided in the MPM because mapping from material point to the grid takes place in each time step to establish updated nodal parameters such as velocity and momentum. The procedures of adding convection and the mapping technique are essentially the same in their effects.

Both LPFDM and MPM, when compared with FEM, have an advantage of easily describing irregular shapes of solids and/or solid inclusions. Any arbitrarily shaped regions in LPFDM or MPM can be filled with irregularly or evenly spaced material points, whereas in FEM, a computationally more demanding meshing has to be performed.

5. CONCLUSIONS

LPFDM (Lagrangian Particle Finite Difference Method) was presented for analyzing large deformations of soils. All the Lagrangian parameters calculated at each time step are carried by Lagrangian points, which represent the material. The numerical examples demonstrated the potential of the Lagrangian particle technique for analyzing large deformations of soils. To allow for more quantitative discussions, appropriate constitutive models for surface soils and the motion of the bedrock beneath the soil deposits must be provided. To do this, future extensions to the method should include implementation of pore water pressure and confining pressure in the PSC tests. To discuss the effects of faulting on tunnels, dams and bridges, a three-dimensional version of the method is necessary and under development.

ACKNOWLEDGMENT: Partial financial supports for this study have been provided by the Japan Society for the Promotion of Science (Grant-

in-Aid for Scientific Research, No. 11875101 and 12355020).

REFERENCES

Brackbill J.U., Ruppel H. M., [1986] "FLIP: A Method for Adaptively Zoned, Particle in Cell Calculations of Fluid Flows in Two Dimensions," *Jour Comput. Phys.*, **65**, 314-343.

Brackbill, J. U., Kothe, D.B. and Ruppel, H.M.,[1988] "'FLIP': A low dissipation, particle-in-cell method," *Jour. Comput. Pys*., **96**, 339-368.

Bray, J. D., [1990] "The effects of Tectonic Movements on Stresses and Deformations in Earth Embankments," *Dissertation Doctor of Philosophy*, University of California, Berkeley, 414.

Burgess D., Sulsky D., Brackbill J.U. [1992] "Mass Matrix Formulation of the FLIP Particle in Cell Method," *J. Comp. Phys*., **103**, 1-15.

Cundall, P. A. [1987] "Distinct Element Models of Rock and Soil Structure," *Analytical and Computational Methods in Engineering Rock Mechanics*, Chapter 4, E.T. Brown, Ed. London: George Allen and Unwin, 129-163.

Cundall, P.A. and Strack, O.D.L. [1979] "A discrete numerical model for granular assemblies," *Geotechnique*, **29**, 47-65.

Harlow, F.H. [1964] "The particle-in-cell computing method for fluid dynamics in fundamental methods in Hydrodynamics," in B. Alder, S. Fernbach and M. Rotenberg (Eds.), *Experimental Arithmetics*, Academic Press, 319-345.

Marti J., Cundall P., Int. Jour. Num. Anal. Meth.Geomech., **6**, 129-139 (1982).

Sulsky, D., Chen, Z., and Schreyer, H.L. [1994] "A particle method for history dependent materials," *Comput. Methods Appl. Mech. Engrg*., **118**, 179-196, 1994.

(Received December 15, 2000)